

# Orbital Effects of In-Plane Magnetic Fields Probed by Mesoscopic Conductance Fluctuations

D. M. Zumbühl,<sup>1</sup> J. B. Miller,<sup>1,2</sup> C. M. Marcus,<sup>1</sup> V. I. Fal'ko,<sup>3</sup> T. Jungwirth,<sup>4,5</sup> and J. S. Harris, Jr.<sup>6</sup>

<sup>1</sup>Department of Physics, Harvard University, Cambridge, Massachusetts 02138

<sup>2</sup>Division of Engineering and Applied Sciences, Harvard University, Cambridge, Massachusetts 02138

<sup>3</sup>Physics Department, Lancaster University, LA1 4YB Lancaster, United Kingdom

<sup>4</sup>Institute of Physics ASCR, Cukrovarnická 10, 162 53 Praha 6, Czech Republic

<sup>5</sup>University of Texas at Austin, Physics Department,

1 University Station C1600, Austin TX 78712-0264

<sup>6</sup>Departement of Electrical Engineering, Stanford University, Stanford, California 94305

We use the high sensitivity to magnetic flux of mesoscopic conductance fluctuations in large quantum dots to investigate changes in the two-dimensional electron dispersion caused by an in-plane magnetic field. In particular, changes in effective mass and the breaking of momentum reversal symmetry in the electron dispersion are extracted quantitatively from correlations of conductance fluctuations. New theory is presented, and good agreement between theory and experiment is found.

PACS numbers: 73.23.Hk, 73.20.Fz, 73.50.Gr, 73.23.-b

A simplified view of transport in a planar two-dimensional conductor, as formed for instance by a semiconductor heterostructure, suggests that when only the lowest quantized subband is occupied, an in-plane magnetic field couples only to the electron spin, allowing the influence of an applied magnetic field to be separated into spin and orbital parts. However, the emerging picture of quantum transport in parallel fields [1, 2, 3] has turned out to be surprisingly rich, indicating that even modest parallel (i.e., in-plane) fields can have significant orbital coupling, break time-reversal symmetry, and generate mesoscopic conductance fluctuations with field-dependent correlations—even without spin-orbit coupling or occupation of higher subbands.

In this Letter, we use the high sensitivity of mesoscopic conductance fluctuations (CF's) to magnetic flux and time-reversal symmetry (TRS) to examine in detail the orbital effects of an in-plane magnetic field,  $B_{\parallel}$ , in a quasiballistic quantum dot formed in a GaAs/AlGaAs 2D electron gas (2DEG). Quantitative comparison of experiment and theory developed here allows the effects of  $B_{\parallel}$  on the electron dispersion in a planar 2DEG, including an anisotropic effective mass and a breaking of TRS (in spatially asymmetric confinement potentials), to be distinguished using various correlation functions of CF's. Effects of nonplanarity of the 2DEG are also included in the theory, and have distinguishable signatures in the CF correlations. The significance of the present work is to demonstrate experimentally that the effects of an in-plane field go far beyond Zeeman coupling, but *cannot* be characterized in terms of simple flux threading through the finite thickness of a 2D electron layer. Also, this study shows that phase coherent CF's can be used as a sensitive quantitative tool, much as one uses a superconducting quantum interference device (SQUID).

Effects of parallel fields on quantum transport have been investigated in 2D systems, including metal films [4], silicon MOSFET's [5], and GaAs/AlGaAs 2DEG's [6, 7], as well as in ballistic focusing geometries [8]. Those

results were mostly interpreted in terms of flux threading due to finite thickness in the confined direction, surface roughness, or deformation of the Fermi circle due to the field. Subband depopulation, decoupling of bilayer systems and diamagnetic shifts caused by  $B_{\parallel}$  have also been observed using cyclotron resonance techniques [9], magnetoresistance measurements [10], and tunneling [11], as well as optical spectroscopy [12]. Related investigations based on quantum-dot weak localization [3] were only sensitive to the breaking of TRS by a parallel field. Here, by using the full CF correlations, the effect of  $B_{\parallel}$  on the full electron dispersion is investigated, and the various

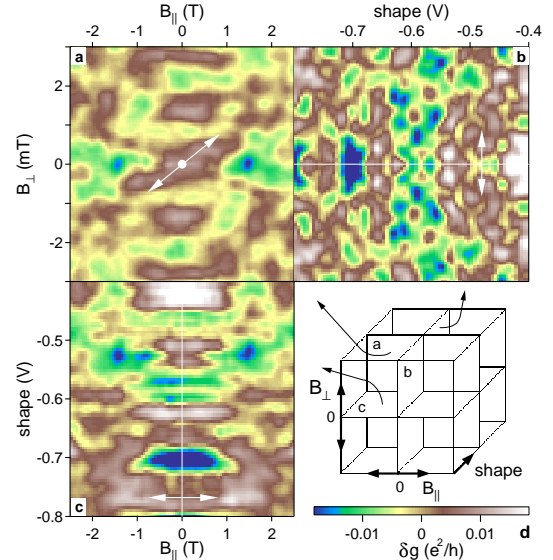


FIG. 1: Conductance fluctuations  $\delta g(B_{\parallel}, B_{\perp}, V) = g(B_{\parallel}, B_{\perp}, V) - \langle g(B_{\parallel}, B_{\perp}, V) \rangle_V$  (color scale) through an  $8 \mu\text{m}^2$  dot with one fully transmitting channel in each lead measured at 0.3K with a) shape-gate voltage  $V = -515 \text{ mV}$ , b)  $B_{\parallel} = 0$  and c)  $B_{\perp} = 0$ , obtained from 2D slices of the three dimensional CF pattern, as indicated in d).

contributions are distinguished.

Two quantum dots, with areas  $A = 8 \mu\text{m}^2$  and  $3 \mu\text{m}^2$ , made on the same wafer, were measured and showed similar behavior. Data from the  $8 \mu\text{m}^2$  dot (see Fig. 3, inset) will be presented in detail. The dots are formed by lateral Cr-Au depletion gates defined by electron-beam lithography on the surface of GaAs/AlGaAs heterostructures grown in the [001] direction. The 2DEG interface is  $900 \text{ \AA}$  below the wafer surface, comprising a  $100 \text{ \AA}$  GaAs cap layer and a  $800 \text{ \AA}$   $\text{Al}_{0.34}\text{Ga}_{0.66}\text{As}$  layer with a  $400 \text{ \AA}$  Si doped layer set back  $400 \text{ \AA}$  from the 2DEG. An electron density of  $n = 2 \times 10^{15} \text{ m}^{-2}$  and bulk mobility  $\mu \sim 14 \text{ m}^2/\text{Vs}$  (cooled in the dark) gives a transport mean free path  $\ell_e \sim 1 \mu\text{m}$ . Note that the  $8 \mu\text{m}^2$  dot contains of order  $10^4$  electrons.

Measurements were made in a  $^3\text{He}$  cryostat at  $0.3 \text{ K}$  using current bias of  $1 \text{ nA}$  at  $338 \text{ Hz}$ . Shape-distorting gates were used to obtain ensembles of statistically independent conductance measurements [13] while the point contacts were actively held at one fully transmitting mode each ( $N = 2$ ). In order to apply tesla-scale  $B_{\parallel}$  while maintaining sub-gauss control of  $B_{\perp}$ , we mount the sample with the 2DEG aligned to the axis of the primary solenoid (accurate to  $\sim 1^\circ$ ) and use an independent split-coil magnet attached to the cryostat to provide  $B_{\perp}$  [14]. The Hall effect measured in a separate GaAs Hall bar mounted next to the quantum dot, as well as the location of weak localization minima in transport through the dot itself (visible  $B_{\parallel} \lesssim 2T$ ) were used to determine the offset in  $B_{\perp}$  (i.e. the residual sample tilt), which was then corrected by computer control of the two independent magnets.

The raw data consist of measured dot conductance  $g(B_{\parallel}, B_{\perp}, V)$  as a function of shape-distorting gate voltage  $V$  (inner loop of multiparameter sweeps),  $B_{\perp}$ , and  $B_{\parallel}$  (outer loop, swept from  $-2.5 \text{ T}$  to  $+4 \text{ T}$  over  $\sim 20 \text{ h}$ ), giving 20 independent shape, 15 independent  $B_{\perp}$  and about 10 independent  $B_{\parallel}$  samples. Conductance fluctuations are found by subtracting the gate-voltage averaged conductance over the measured range:  $\delta g(B_{\parallel}, B_{\perp}, V) = g(B_{\parallel}, B_{\perp}, V) - \langle g(B_{\parallel}, B_{\perp}, V) \rangle_V$ .

Figure 1 shows 2D slices of conductance fluctuations in the full 3D space of  $B_{\parallel}$ ,  $B_{\perp}$ , and  $V$ . Note that because gate-voltage-averaged conductance is subtracted from the fluctuations, weak localization effects on  $\langle g \rangle$  are not evident in Fig. 1. A principal result is already evident in Fig. 1: The horizontally elongated features around  $|B_{\parallel}| \sim 0$  in Fig. 1(c) show qualitatively that CF's are less sensitive to  $B_{\parallel}$  in the vicinity of  $|B_{\parallel}| \sim 0$ , giving a larger correlation field near  $|B_{\parallel}| \sim 0$ , than at larger parallel fields. This elongation, demonstrating reduced flux sensitivity near  $|B_{\parallel}| \sim 0$ , is consistent with the  $B_{\parallel}$  dependent effective mass and momentum reversal symmetry breaking terms of our theory. Effects of nonplanarity alone would result in a  $B_{\parallel}$  independent correlation field. A quantitative analysis is presented in Fig. 2.

The 2D slices in Fig. 1 also illustrate the fundamental symmetries of conductance with respect to magnetic

fields  $B_{\parallel}$  and  $B_{\perp}$ : when  $B_{\parallel} = 0$ , conductance is symmetric under inversion of  $B_{\perp}$ ,  $g(B_{\perp}) = g(-B_{\perp})$  (see Fig. 1(b)); when  $B_{\perp} = 0$ , conductance is symmetric under inversion of  $B_{\parallel}$ ,  $g(B_{\parallel}) = g(-B_{\parallel})$  (see Fig. 1(c)). When both  $B_{\parallel}$  and  $B_{\perp}$  are nonzero, the symmetry of conductance requires the reversal of both fields,  $g(B_{\parallel}, B_{\perp}) = g(-B_{\parallel}, -B_{\perp})$  (see Fig. 1(a)) [15]. The fact that a nonzero  $B_{\parallel}$  breaks the symmetry  $g(B_{\perp}) = g(-B_{\perp})$  is a simple qualitative demonstration that  $B_{\parallel}$  breaks TRS [3]. A quantitative analysis of this effect is presented in Fig. 3.

To quantify the correlations of the various parameters used to generate CF's — including in particular  $B_{\parallel}$  — we define the normalized correlation functions,

$$C_v(B_{\parallel}) = \frac{\langle \delta g(B_{\parallel}, V) \delta g(B_{\parallel}, V + v) \rangle}{\langle \delta g^2(B_{\parallel}) \rangle} \quad (1)$$

$$C_{b_{\perp}}(B_{\parallel}) = \frac{\langle \delta g(B_{\parallel}, B_{\perp}) \delta g(B_{\parallel}, B_{\perp} + b_{\perp}) \rangle}{\langle \delta g^2(B_{\parallel}) \rangle} \quad (2)$$

$$C_{b_{\parallel}}(B_{\parallel}) = \frac{\langle \delta g(B_{\parallel}) \delta g(B_{\parallel} + b_{\parallel}) \rangle}{\sqrt{\langle \delta g^2(B_{\parallel}) \rangle \langle \delta g^2(B_{\parallel} + b_{\parallel}) \rangle}}, \quad (3)$$

where  $\langle \dots \rangle$  is shorthand for  $\langle \dots \rangle_{V, B_{\perp}}$ , i.e., averaging over both gate voltage and  $B_{\perp}$ , with  $B_{\perp}$  sufficiently large to fully break TRS throughout the measured range.

Theoretical expressions for the correlation functions in Eqs. 1–3 can be found using the effective 2D Hamiltonian

$$\hat{H}_{2D} = \frac{\mathbf{p}^2}{2m} - p_{\perp}^2 \gamma(B_{\parallel}) + p_{\parallel}^2 \beta(B_{\parallel}) + u(\mathbf{r}), \quad (4)$$

for electrons confined to a plane perpendicular to  $\hat{z}$  [1]. Here,  $\mathbf{p} = -i\hbar\nabla - \frac{e}{c}\mathbf{A}_{2D}$ , with  $\text{rot}\mathbf{A}_{2D} = B_{\perp}$ , is the 2D momentum operator in the plane, with component  $p_{\perp} = \vec{p} \cdot [\vec{B}_{\parallel} \times \vec{l}_z] / B_{\parallel}$  perpendicular to  $B_{\parallel}$ , and  $u(\mathbf{r})$  is the impurity and dot confining potential. The middle terms in  $\hat{H}_{2D}$  arise from  $p_{\perp}$ -dependent subband mixing: the  $\gamma(B_{\parallel})$  term lifts rotational symmetry with an anisotropic mass enhancement [7] but does not break TRS; the  $\beta(B_{\parallel})$  arises from the broken spatial inversion symmetry of the heterointerface and breaks TRS in presence of  $B_{\parallel}$ .

Extending the analysis of Ref. [1] to higher temperature yields a correlation between conductance fluctuations at  $B_{\parallel}$  and at  $B_{\parallel} + b_{\parallel}$  of the form

$$C_{b_{\parallel}}(B_{\parallel}) = \left[ 1 + \frac{\tau_d^{-1}(B_{\parallel}, b_{\parallel})}{\tau_{esc}^{-1}} \right]^{\alpha}, \quad (5)$$

in the unitary ensemble, where  $\tau_{esc}^{-1} = N\Delta/h$  is the escape rate from the dot, with  $\Delta = 2\pi\hbar^2/m^*A$  the mean level spacing of the corresponding closed dot (effective electron mass  $m^* = 0.067m_e$ ),  $\tau_d^{-1}$  is an additional escape rate due to orbital effects of  $B_{\parallel}$ , as discussed below. The exponent  $\alpha$  equals  $-1$  in the high temperature limit  $kT \gg (\hbar\tau_{esc}^{-1}, \hbar\tau_d^{-1}, \epsilon_Z)$ , applicable in the present experiment, and  $-2$  in the low temperature limit, where  $\epsilon_Z = g\mu_B B$  is the Zeeman energy, with  $g = -0.44$  for

GaAs. The difference between the high and low temperature regimes is caused by the necessity to average the interference contributions coming from electrons at different energies. For parallel fields with  $\epsilon_Z \lesssim 3kT$ , appropriate for the present measurements, the deviation of Eq. (5) from the full expression is negligible [16].

The additional escape rate  $\tau_d^{-1}$  due to  $B_{\parallel}$  is given by

$$\tau_d^{-1}(B_{\parallel}, b_{\parallel}) = \frac{\tau p_F^4}{8\hbar^2} [\gamma(B_{\parallel}) - \gamma(B_{\parallel} + b_{\parallel})]^2 \quad (6)$$

$$+ \frac{\tau p_F^6}{8\hbar^2} \left[ \frac{\beta(B_{\parallel}) - \beta(B_{\parallel} + b_{\parallel})}{2} \right]^2 + \frac{\zeta^2 p_F^2}{2\tau} b_{\parallel}^2,$$

where  $\tau = \mu m^*/e$  is the elastic scattering time in a diffusive dot or the crossing time  $\tau = m^*L/p_F$  in a ballistic device, where  $L$  is the diameter of the device and  $p_F = \hbar(2\pi n)^{1/2}$  is the Fermi momentum. The  $\zeta$  term describes effects of nonplanarity, including interface roughness and dopant inhomogeneities, and also breaks TRS.

Writing the functions  $\gamma(x)$  and  $\beta(x)$  in Eq. (6) in terms of scale factors  $\tilde{\gamma}$  and  $\tilde{\beta}$  and normalized functions  $g(x)$  and  $f(x)$  as  $\gamma(x) = \tilde{\gamma}g(x)$  and  $\beta(x) = \tilde{\beta}f(x)$ , we find  $g(x)$  and  $f(x)$  from self-consistent simulations of the heterostructure [17] and treat  $\tilde{\gamma}$  and  $\tilde{\beta}$  as fit parameters. Below  $\sim 2$  T, the normalized functions are well approximated by  $g(x) \approx x^2$  and  $f(x) \approx x^3$  (see Fig. 2(b), insets); however, the full functions are used for all comparison of theory and experiment. We note that  $\tilde{\gamma}$  and  $\tilde{\beta}$  can also be obtained from the heterostructure simulations, giving values in reasonable agreement with those obtained from the fits.

Figure 2(a) shows experimental correlation functions,  $C_{b_{\parallel}}$ ,  $C_{b_{\perp}}$ , and  $C_v$ , for representative parallel fields, as indicated. The corresponding characteristic voltage  $v^c$  and fields  $b_{\perp}^c$  and  $b_{\parallel}^c$  are shown in Fig. 2(b) as a function of  $B_{\parallel}$ , as obtained from the half width at half maximum (HWHM) values of the correlation functions, indicated by dashed lines in Fig. 2(a). It is evident from Fig. 2(b) that both  $b_{\perp}^c$  and  $v^c$  are independent of  $B_{\parallel}$  within the error bars, in agreement with theory and previous experiments [14]. (An alternative procedure, not shown, for extracting these same quantities from the slopes of log-power spectra of CF's yields similar values for  $v^c$  and  $b_{\parallel}^c$  that are again independent of  $B_{\parallel}$ , within error bars.)

In contrast, the parallel field correlation length,  $b_{\parallel}^c$ , shown in Fig. 2(b) decreases substantially from its zero-field value on a field scale of  $\sim 1$  T. Good agreement with theory is found: the solid curve in Fig. 2(b) is the best-fit (described below) theoretical HWHM correlation field for  $C_{b_{\parallel}}(B_{\parallel})$  obtained from Eq. (5). This decrease is due to the  $\gamma$  and  $\beta$  terms in Eq. (6) and cannot be accounted for with the  $\zeta$  term alone.

Symmetries of conductance in parallel and perpendicular fields are investigated in Fig. 3. We define the cross-correlation functions

$$C_{\pm\pm}(B_{\parallel}) = \frac{\langle \delta g(B_{\parallel}, B_{\perp}) \delta g(\pm B_{\parallel}, \pm B_{\perp}) \rangle}{\sqrt{\langle \delta g^2(B_{\parallel}, B_{\perp}) \rangle \langle \delta g^2(\pm B_{\parallel}, \pm B_{\perp}) \rangle}}. \quad (7)$$

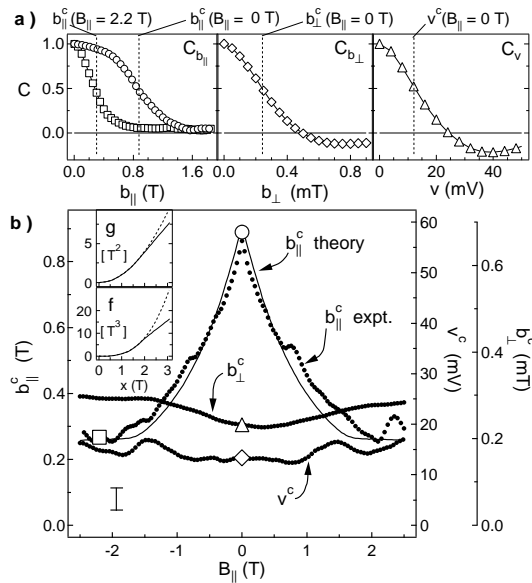


FIG. 2: a) Correlation functions  $C_{b_{\parallel}}$  at  $B_{\parallel} = 0, 2.2$  T (open circles, squares) as well as  $C_{b_{\perp}}$  (open diamonds) and  $C_v$  (open triangles) at  $B_{\parallel} = 0$ . Half width at half maximum values give the characteristic voltage  $v^c$  and fields  $b_{\perp}^c$  and  $b_{\parallel}^c$ , shown in b) (solid circles) as a function of  $B_{\parallel}$ . Markers in b) refer to corresponding curves in a). The solid curve shows the three-parameter theory. A typical error bar is indicated. Insets:  $g(x)$  and  $f(x)$  used for fits (see text) as obtained from numerical simulations (solid curves) as well as quadratic and cubic low field approx. (dashed curves).

With this definition, the first (second) subscript index of  $C$  refers to whether  $B_{\parallel}(B_{\perp})$  is reversed when computing the correlation function. Correlations for total field reversal,  $C_{--}$  (i.e., both  $B_{\parallel}$  and  $B_{\perp}$  inverted) remain near unity for all parallel fields, as expected from the full Landauer-Büttiker (Onsager) symmetry (see Fig. 3(a)). Deviations from a perfect correlation  $C_{--} = 1$  are small, indicating that the confining potential of the dot did not drift significantly over periods of a day. Figure 3(a) also shows conductance fluctuations at  $(B_{\parallel}, B_{\perp})$  and  $(B_{\parallel}, -B_{\perp})$  ( $C_{+-}$ ) become uncorrelated ( $C_{+-} \sim 0$ ) at parallel fields of a few tesla, indicating the field scale at which  $B_{\parallel}$  breaks TRS. Within error bars,  $C_{-+}$  is indistinguishable from  $C_{+-}$ , as expected from Landauer-Büttiker symmetry,  $\delta g(-B_{\parallel}, B_{\perp}) = \delta g(B_{\parallel}, -B_{\perp})$ . The theoretical cross-correlation using Eq. (5), shown as a solid curve in Fig. 3(a), is in very good agreement with experiment data.

Finally, we discuss the full correlation,  $C_{b_{\parallel}}(B_{\parallel})$ , of CF's at  $B_{\parallel}$  with CF's at  $B_{\parallel} + b_{\parallel}$ . Representative curves for  $B_{\parallel} = 0, 0.6, 1, 1.4$  T are shown in the lower part of Fig. 3 as a function of  $B_{\parallel} + b_{\parallel}$ , along with best-fit theory curves based on Eq. (5). Besides the perfect correlation at  $b_{\parallel} = 0$  ( $C_{b_{\parallel}=0} = 1$ ), there is an “echo” of correlations, both in experiment and theory, that occurs at  $b_{\parallel} \sim -2B_{\parallel}$ . Within the present theory, this field-reversed correlation “echo”,  $C_{-2B_{\parallel}}$ , is suppressed from

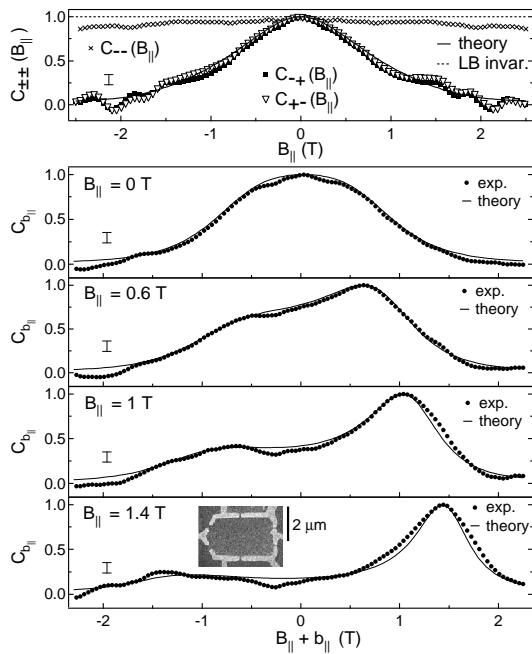


FIG. 3: Top: Cross-correlations of CF's at  $(B_{\parallel}, B_{\perp})$  with CF's at  $(-B_{\parallel}, -B_{\perp})$  ( $C_{--}$ , crosses),  $(-B_{\parallel}, B_{\perp})$  ( $C_{-+}$ , squares) and  $(B_{\parallel}, -B_{\perp})$  ( $C_{+-}$ , triangles) as a function of  $B_{\parallel}$ . Landauer-Büttiker (LB) symmetry for full field reversal gives  $C_{--} = 1$  (Dashed line). Below: Correlation functions  $C_{b_{\parallel}}(B_{\parallel})$  at  $B_{\parallel} = 0, 0.6, 1, 1.4$  T. Solid curves show theory based on Eq. (5). Typical error bars as indicated.

unity only to the extent that parallel field breaks TRS. The agreement between theory and experiment, including the unusual asymmetric curves in Fig. 3, is quite good. A single, consistent set of three parameters ( $\tilde{\gamma}$ ,  $\tilde{\beta}$ ,

$\zeta$ ) have been obtained from fits of Eq. (5) to 131 curves like those in Fig. 3, ranging over  $-2.5 \text{ T} \leq B_{\parallel} \leq 4 \text{ T}$ . We emphasize that *all* theory curves shown in Fig. 2 and Fig. 3 used this single set of three fit parameters and were not individually fit. The values obtained in this way were  $\tilde{\gamma} = 11 \pm 2 \times 10^{-4} [m^*]^{-1} T^{-2}$ ,  $\tilde{\beta} = 4 \pm 4 \times 10^{-4} [m^* p_F]^{-1} T^{-3}$ , and  $\zeta = 44 \pm 8 \times 10^{-3} [p_F]^{-1} T^{-1}$ , consistent within the error bars with values extracted for the  $3 \mu\text{m}^2$  dot. We note that parameters  $\tilde{\beta}$  and  $\zeta$  obtained from the parallel-field-induced crossover from the orthogonal to the unitary ensemble [3] are in good agreement. The self-consistent simulations give theoretical values of  $\tilde{\gamma} = 35 \times 10^{-4} [m^*]^{-1} T^{-2}$ ,  $\tilde{\beta} = 3 \times 10^{-4} [m^* p_F]^{-1} T^{-3}$ .

In summary, orbital effects of an in-plane magnetic field  $B_{\parallel}$  were experimentally investigated using the high sensitivity of CF's to magnetic flux in a large quasiballistic quantum dot. Detailed quantitative comparison of correlations of CF's induced by  $B_{\parallel}$  with theory developed here reveal the mechanisms of coupling, including an induced anisotropic effective mass, the breaking of time-reversal symmetry due to the heterostructure asymmetry and effects of nonplanarity. In the present experiment, spin-orbit coupling is weak. On the other hand, the combined influence of stronger spin-orbit coupling [3] and parallel fields is expected to yield interesting additional features in the correlations and symmetries of CF's [18]. These remain to be investigated experimentally.

We thank I. Aleiner, P. Brouwer, J. Folk and D. Goldhaber-Gordon for useful discussions. This work was supported in part by DARPA-QuIST, DARPA-SpinS, ARO-MURI and NSF-NSEC. Work at UCSB was supported by QUEST, an NSF Science and Technology Center. JBM acknowledges partial support from NDSEG, and VIF from the Royal Society and EPSRC.

- 
- [1] V. I. Fal'ko and T. Jungwirth, Phys. Rev. B **65**, 81306 (2002).  
[2] J. S. Meyer, A. Altland and B. L. Altshuler, Phys. Rev. Lett. **89**, 206601 (2002); J. S. Meyer, V. I. Fal'ko and B. L. Altshuler, in NATO Science Series II, Vol. 72, edited by I.V. Lerner, B.L. Altshuler, V.I. Fal'ko and T. Giamarchi (Kluwer Academic Publishers, Dordrecht, 2002), pp. 117-164.  
[3] D. M. Zumbühl, J. B. Miller, C. M. Marcus, K. Campman, and A. C. Gossard, Phys. Rev. Lett. **89**, 276803 (2002); D. M. Zumbühl *et al.*, (to be published).  
[4] Z. Ovadyahu *et al.*, Phys. Rev. B **32**, 781 (1985); N. Giordano and M. A. Pennington, Phys. Rev. B **47**, 9693 (1993).  
[5] D. J. Bishop *et al.*, Phys. Rev. B **26**, 773 (1982); P. M. Mensz and R. G. Wheeler, Phys. Rev. B **35**, 2844 (1987); U. Kunze, Phys. Rev. B **35**, 9168 (1987).  
[6] B. J. F. Lin *et al.*, Phys. Rev. B **29**, 927 (1984).  
[7] J. M. Heisz and E. Zaremba, Phys. Rev. B **53**, 13594 (1996).  
[8] K. Ohtsuka *et al.*, Physica B **249-251**, 780 (1998); K. Oto *et al.*, Physica E **11**, 177 (2001).  
[9] Z. Schlesinger *et al.*, Phys. Rev. Lett. **50**, 2098 (1983).  
[10] D. R. Leadley *et al.*, Semicond. Sci. Technol. **5**, 1081 (1990); J. J. Mares *et al.*, Phys. Rev. Lett. **80**, 4020 (1998); O. N. Makarovskii *et al.*, Phys. Rev. B **62**, 10908 (2000); P. Svoboda *et al.*, Physica E **12**, 315 (2002).  
[11] K. K. Choi *et al.*, Phys. Rev. B **38**, 12362 (1988).  
[12] D. C. Reynolds *et al.*, Phys. Rev. B **35**, 4515 (1987); V. Kirpichev *et al.*, JETP Lett. **51**, 436 (1990); I. Kukushkin *et al.*, JETP Lett. **53**, 334 (1991).  
[13] C. M. Marcus *et al.*, Phys. Rev. Lett. **69**, 506 (1992); I. H. Chan *et al.*, Phys. Rev. Lett. **74**, 3876 (1995); A. G. Huibers *et al.*, Phys. Rev. Lett. **81**, 1917 (1998).  
[14] J. A. Folk *et al.*, Phys. Rev. Lett. **86**, 2102 (2001).  
[15] M. Büttiker and Y. Imry, J. Phys. C. **L**, 467 (1985).  
[16] V. I. Fal'ko and T. Jungwirth, unpublished.  
[17] The simulations take into account band offsets, Hartree and exchange-correlation potentials as well as the potential due to residual acceptor impurities, as obtained from the onset of second subband population.  
[18] J. H. Cremers, P. W. Brouwer and V. I. Fal'ko, condmat/0304222; I. Aleiner and V. I. Fal'ko, Phys. Rev. Lett. **87**, 256801 (2001).